mathematics

MDPI

Article

A Novel Nonsingular Terminal Sliding Mode Observer-Based Sensorless Control for Electrical Drive System

Yongjie Yang [1] and Xudong Liu [1,2,*]

[1] College of Automation, Qingdao University, Qingdao 266071, China
[2] Shandong Key Laboratory of Industrial Control Technology, Qingdao 266071, China
* Correspondence: lxd2017@qdu.edu.cn

Abstract: To improve the sensorless control performance of electrical drive systems, a nonsingular terminal sliding mode observer (NTSMO) and adaptive observer are proposed to solve the chattering and phase delay problems. Firstly, by defining a new nonsingular terminal sliding mode surface, the sliding mode observer based on the fast reaching law is designed to estimate the back electromotive force (EMF). The observer enhances the robustness and system performance eliminates the singularity and attenuates the chattering. Next, to obtain the accurate back-EMF signal, an adaptive observer is designed instead of a traditional low-pass filter to filter out the harmonics. The adaptive observer can avoid the phase delay problem and further improve the signal observation accuracy. Then, the rotor position and speed information are accurately tracked. The proposed method is applied to the speed control system of a permanent magnet synchronous motor (PMSM), and the effectiveness and feasibility of the proposed sliding mode observer are demonstrated by the experiment.

Keywords: permanent magnet synchronous motor; nonsingular terminal sliding mode observer; adaptive observer

MSC: 93A30

Citation: Yang, Y.; Liu, X. A Novel Nonsingular Terminal Sliding Mode Observer-Based Sensorless Control for Electrical Drive System. *Mathematics* **2022**, *10*, 3123. https://doi.org/10.3390/math10173123

Academic Editors: Rongwei Guo, Cuimei Jiang and Ruimin Xu

Received: 2 August 2022
Accepted: 29 August 2022
Published: 31 August 2022

1. Introduction

Permanent magnet synchronous motor (PMSM) has the characteristics of high power density, high efficiency, and high reliability [1], and it is widely used in industrial applications [2]. The advanced technologies based on vector control or direct torque control are often used in the field of high-performance electrical drive systems, and the rotor position and speed information are usually obtained by installing an encoder or resolver [3,4]; however, the use of mechanical sensors will increase the size and cost of the motor drive system; therefore, the sensorless speed control technologies of PMSM have received extensive attention [5,6].

According to the running speed of the motor, the sensorless control strategies of PMSM can be divided into two categories. One is the high-frequency signal injection method, which does not depend on the model of the motor, but is easily affected by high-frequency noise. It is suitable for the zero low-speed range [7,8]. The other is sensorless control based on back electromotive force (EMF) [9,10]. The back-EMF is estimated by the model of the motor, and the speed and position are further calculated. Because it is difficult to derive the accurate back-EMF at a low speed, this method is usually applied in the medium and high-speed range. Recently, a lot of sensorless methods based on back-EMF have been proposed, such as the sliding mode observer [11,12], model reference adaptive control [13], flux linkage observation [14], and Kalman filter observer [15].

Among these methods, because of its low requirements on the model of the control system, the sliding mode observer (SMO) is widely used in sensorless control of electrical drive systems [16,17]. Sliding mode control is usually divided into two parts, one is sliding mode surface design and the other is reaching law control [18]. The reaching law control is directly related to the process of reaching the sliding surface. Sliding mode control (SMC) is a kind of variable structure control, which has the advantages of fast convergence speed and strong robustness [19]. Although SMC has attractive advantages, it has an inherent feature of chattering may hinder its application; therefore, it is a challenge to suppress chattering in sliding mode control [20,21]. Considering the influence of VSI nonlinearity, in [22], an adaptive super-twisting algorithm-based sliding mode observer (STA-SMO) is proposed to estimate the speed and position information. Compared with conventional sliding mode observer, the estimation accuracy is improved and the speed estimation accuracy is improved. To solve the delay problem existing in SMO, a hyperbolic function is proposed in [23] as a switching function to solve the delay problem. In [24], a sensorless speed control approach of the induction motor applying full-order terminal sliding mode (FOTSM) control theory is proposed, and the accuracy of the sensorless control system is improved. To reduce the chattering effect and improve control accuracy, an improved sliding mode observer by redesigning the sliding switching function is designed for surface-mounted PMSM; through the introduction of an intermediate variable, the back-EMF is extended at a low speed [25]. To suppress the estimated position error, a full-order sliding mode observer with a novel phase-locked loop is designed in [26] for sensorless control of PMSM. In [27], a novel adaptive-gain SMO is designed for sensorless control, and the gain can dynamically adapt to a changing operation condition. In [28], a super-twisting sliding mode observer (STSMO) is proposed to realize high-performance sensorless control. The effectiveness of this method is verified by experiments and simulations.

In this paper, to improve the control accuracy of the sensorless speed control system, a composite control method based on a nonsingular terminal sliding mode observer and an adaptive observer is proposed. Compared with the conventional sliding mode observer to achieve sensorless control, the method designed in this paper can further reduce the chattering problem of the system, improve the observation accuracy, and effectively improve the system performance. Moreover, compared with STSMO [28], the observer structure designed in this paper is simpler, and the chattering problem of the system is further suppressed. The experimental results show that the method can effectively improve the observation accuracy and anti-disturbance performance. The main contributions are as follows.

(1) A nonsingular terminal sliding mode observer is designed for the sensorless speed control of PMSM by using an improved sliding mode reaching law. The estimation accuracy of the speed is improved.
(2) An adaptive observer is used to replace the low-pass filter in the conventional sliding mode observer, which effectively avoids the phase delay problem and further improves the observation accuracy.
(3) The stability of the system is proved by the Lyapunov function. Compared with the conventional SMO and super-twisting SMO, the experimental results show that the proposed method can improve the observation accuracy of the speed and effectively reduce the chattering.

This paper is organized as follows. In Section 2, a sliding mode observer for permanent magnet synchronous motor is designed, which includes conventional sliding mode observer and nonsingular terminal sliding mode observer. In addition, the new reaching law used is numerically simulated, and the stability of the designed observer is verified by Lyapunov function. Experiments are verified in Section 3. Conclusions are provided in Section 4.

2. Design of the Observer

2.1. Conventional Sliding Mode Observer

The mathematical model of the surface-mounted PMSM in two-phase stationary coordinate system can be represented as [29]

$$\begin{cases} \frac{d}{dt} i_\alpha = -\frac{R_s}{L_s} i_\alpha + \frac{1}{L_s} u_\alpha - \frac{1}{L_s} e_\alpha \\ \frac{d}{dt} i_\beta = -\frac{R_s}{L_s} i_\beta + \frac{1}{L_s} u_\beta - \frac{1}{L_s} e_\beta \end{cases} \tag{1}$$

$$\begin{cases} e_\alpha = -\psi_f \omega_e \sin\theta_e \\ e_\beta = \psi_f \omega_e \cos\theta_e \end{cases} \tag{2}$$

where i_α, i_β are the phase currents in the stationary reference frame. u_α, u_β are the phase voltages in the stationary reference frame. e_α, e_β are the back-EMF components of the shaft. L_s, R_s are the stator inductance and stator resistance, respectively. ψ_f is the permanent magnet flux linkage. ω_e is the rotor electrical angular velocity. θ_e is the rotor electrical angle position.

According to the sensorless control method of permanent magnet synchronous motor based on sliding mode observer [30], the sliding mode surface is defined as

$$s(x) = \begin{pmatrix} \tilde{i}_\alpha \\ \tilde{i}_\beta \end{pmatrix} = \begin{pmatrix} \hat{i}_\alpha - i_\alpha \\ \hat{i}_\beta - i_\beta \end{pmatrix} \tag{3}$$

where $\tilde{i}_\alpha$ and $\tilde{i}_\beta$ are the current estimation errors. $\hat{i}_\alpha$ and $\hat{i}_\beta$ are the estimation values of the phase currents.

Then, the sliding mode observer is usually designed as

$$\begin{cases} \frac{d}{dt} \hat{i}_\alpha = -\frac{R_s}{L_s} \hat{i}_\alpha + \frac{1}{L_s} u_\alpha - \frac{1}{L_s} v_\alpha \\ \frac{d}{dt} \hat{i}_\beta = -\frac{R_s}{L_s} \hat{i}_\beta + \frac{1}{L_s} u_\beta - \frac{1}{L_s} v_\beta \end{cases} \tag{4}$$

where v_α and v_β represent the control functions of the sliding mode observer.

Subtract (1) from (4), the differential of current estimation errors can be obtained as

$$\frac{d}{dt}\begin{bmatrix} \tilde{i}_\alpha \\ \tilde{i}_\beta \end{bmatrix} = -\frac{R_s}{L_s}\begin{bmatrix} \tilde{i}_\alpha \\ \tilde{i}_\beta \end{bmatrix} + \frac{1}{L_s}\begin{bmatrix} e_\alpha - v_\alpha \\ e_\beta - v_\beta \end{bmatrix} \tag{5}$$

Next, the sliding mode control law is designed as

$$\begin{bmatrix} v_\alpha \\ v_\beta \end{bmatrix} = \begin{bmatrix} k_1 \mathrm{sgn}(\hat{i}_\alpha - i_\alpha) \\ k_1 \mathrm{sgn}(\hat{i}_\beta - i_\beta) \end{bmatrix} \tag{6}$$

where, k_1 is the SMO gain and $k_1 > 0$. If the value of k_1 is too large, the chattering of the system will increase. If the value of k_1 is too small, the dynamic performance of the system will be affected.

According to the equivalent control principle of sliding mode [31], the back-EMF is derived as

$$\begin{bmatrix} e_\alpha \\ e_\beta \end{bmatrix} = \begin{bmatrix} v_\alpha \\ v_\beta \end{bmatrix} = \begin{bmatrix} k_1 \mathrm{sgn}(\tilde{i}_\alpha) \\ k_1 \mathrm{sgn}(\tilde{i}_\beta) \end{bmatrix} \tag{7}$$

Since the estimated back-EMF contains higher harmonics, it is usually filtered with a low-pass filter [32]. Rotor position and speed information can be calculated from the filtered back-EMF. Considering the delay of the low-pass filter, certain phase compensation is required. The estimated rotor position and speed after compensation are

$$\hat{\theta}_e = -\arctan\frac{\hat{e}_\alpha}{\hat{e}_\beta} + \Delta\theta_e \tag{8}$$

$$\hat{\omega}_e = \frac{\sqrt{\hat{e}_\alpha + \hat{e}_\beta}}{\psi_f} \tag{9}$$

where $\hat{e}_\alpha$, $\hat{e}_\beta$ are α-axis and β-axis estimation of back-EMF. $\hat{\theta}_e$ is the estimation of electrical angle. $\hat{\omega}_e$ is the estimation of electrical angular velocity. $\Delta\theta = \arctan(\hat{\omega}_e/\omega_c)$ is to compensate for the angle of the rotor. w_c is the cutoff frequency of the low-pass filter. For different rotational speeds and cut-off frequencies, the compensation angles are different.

2.2. Design of Nonsingular Terminal Sliding Mode Observer

In order to achieve good performances, such as fast convergence and better tracking precision, the nonsingular terminal sliding surface is designed as [33]

$$s(t) = \tilde{i}(t) + \beta \int_0^t \left|\tilde{i}(\tau)\right|^\lambda \mathrm{sgn}(\tilde{i}(\tau)) d\tau \tag{10}$$

where $\beta > 0$, $\lambda = p/q$, p, and q are positive odd integers and $0 < \lambda < 1$, $\left|\tilde{i}(\tau)\right|^\lambda \mathrm{sgn}(\tilde{i}(\tau))$ is defined as $\left|\tilde{i}(\tau)\right|^\lambda \mathrm{sgn}(\tilde{i}(\tau)) = \begin{bmatrix} \left|\tilde{i}_\alpha(\tau)\right|^\lambda \mathrm{sgn}(\tilde{i}_\alpha(\tau)) & \left|\tilde{i}_\beta(\tau)\right|^\lambda \mathrm{sgn}(\tilde{i}_\beta(\tau)) \end{bmatrix}^T$.

Let $\dot{x}_I(t) = |x(t)|^\lambda \mathrm{sgn}(x(t))$ and $x_I(0) = -x(0)/\beta$, when the system moves on an ideal sliding surface, it can be obtained $x(t) = -\beta x_I(t)$ and $\dot{x}_I(t) = -\beta|x_I(t)|^\lambda \mathrm{sgn}(x_I(t))$. The finite time of $x(t)$ from $x(0)$ to $x\left(t_f\right)$ is the same as the finite time of $x_I(t)$ from $x_I(0)$ to $x_I\left(t_f\right) = 0$. From Equation (10), it can be calculated as $t_f = \beta^{-1}(1-\lambda)^{-1}|x(0)|^{1-\lambda}$, so the observer can converge to a steady-state in a finite time.

When the system reaches the sliding mode surface, then $s = \dot{s} = 0$, the following can be obtained from (10) as

$$\dot{\tilde{i}} + \beta\left|\tilde{i}\right|^\lambda \mathrm{sgn}\tilde{i} = 0 \tag{11}$$

Then

$$\dot{\tilde{i}} = -\beta\left|\tilde{i}\right|^\lambda \mathrm{sgn}\tilde{i} \tag{12}$$

The sliding mode control law usually consists of equivalent control and switching control [34]. According to the model of current estimation errors (5) and the sliding mode surface (10), the sliding mode control law is designed as

$$\begin{cases} v = v_{eq} + v_{sw} \\ v_{eq} = R_s\tilde{i} - L_s\beta\left|\tilde{i}\right|^\lambda \mathrm{sgn}\tilde{i} \\ v_{sw} = -\frac{k}{\xi+\sigma^{|s|}}|s|^\varpi \mathrm{sgn}(s) - \frac{\varepsilon}{\xi+\sigma^{|s|}}s \end{cases} \tag{13}$$

where $0 < \xi < 1$, $0 < \sigma < 0.1$, $0 < \varpi < 1$, $k > 0$. v_{eq} is the equivalent control. v_{sw} is the switch control, and it can also be seen as sliding mode reaching law. The equivalent control rate is obtained without considering the back-EMF.

The back-EMF can be observed as

$$e = v = v_{eq} + v_{sw} \tag{14}$$

To ensure the stability of the system, the Lyapunov function is selected [35]

$$V = s^2/2 \tag{15}$$

The derivation of V can be expressed as

$$\begin{aligned}
&\dot{V}{=}s\dot{s} \\
&= s\left(\dot{\tilde{i}} + \beta|\tilde{i}|^{\lambda} sgn\tilde{i}\right) \\
&{=}s\left[\left(-R_s\tilde{i} + v + e\right)/L + \beta|\tilde{i}|^{\lambda} sgn\tilde{i}\right] \\
&= 1/Ls\left(e - \frac{k}{\xi+\sigma^{|s|}}|s|^{\varpi}\mathrm{sgn}(s) - \frac{\varepsilon}{\xi+\sigma^{|s|}}s\right) \\
&{=}1/L\left(se - \frac{k}{\xi+\sigma^{|s|}}|s|^{\varpi+1} - \frac{\varepsilon}{\xi+\sigma^{|s|}}s^2\right) \\
&\leq\ 1/L\left(|s||e| - \frac{k}{2}|s|^{\varpi+1} - \frac{\varepsilon}{2}|s|^2\right)
\end{aligned} \tag{16}$$

Beyond $|s| \leq \min\left((2|e|/k)^{1/\varpi}, 2|e|/\varepsilon\right)$, $\dot{V}$ is negative definite. The solution starting inside $V \leq c$ remain inside it at all future times, where $c > 1/2\left(min\left((2|e|/k)^{1/\varpi}, 2|e|/\varepsilon\right)\right)^2$, since $\dot{V}$ is negative on the boundary $V = c$, and hence the solution is uniformly bounded.

To filter the high-frequency noise signal and solve the phase delay problem of the low pass filter, an adaptive observer is designed to derive the accurate back-EMF. Assuming that the motor speed is constant within an estimation period. According to (2), the differential of the back-EMF can be expressed as [28]

$$\begin{cases} \frac{de_\alpha}{dt} = -\omega e_\beta \\ \frac{de_\beta}{dt} = \omega e_\alpha \end{cases} \tag{17}$$

The adaptive observer is designed as

$$\begin{cases} \frac{d\hat{e}_\alpha}{dt} = -\widehat{\omega}\hat{e}_\beta - k_3(\hat{e}_\alpha - e_\alpha) \\ \frac{d\hat{e}_\beta}{dt} = -\widehat{\omega}\hat{e}_\alpha - k_4(\hat{e}_\beta - e_\beta) \end{cases} \tag{18}$$

where k_3 and k_4 are observer gains, and $k_3 > 0$, $k_4 > 0$. The adaptive observer has good robustness and can effectively filter high-frequency noise to obtain accurate back-EMF signal. The phase delay problem caused by the traditional filter is avoided.

Finally, the motor speed and position can be estimated from (9) and (19).

$$\hat{\theta}{=}\int \hat{\omega}_e dt \tag{19}$$

The system structure is shown in Figure 1. The control system includes an interior mounted PMSM, an inverter, a pulse width modulation (PWM) module, two coordinate transformation modules, the PI speed controller, the PI current controller, the nonsingular terminal sliding mode observer, and the adaptive obvserver. ω^* is the reference speed. The d-axes reference current ${i_d}^*$ is usually set to zero to ensure a constant flux operating condition. The nonsingular terminal sliding mode observer is used to estimate the motor back-EMF, and the adaptive observer is used to filter the back-EMF signal and estimate the motor speed information and rotor position information, so as to realize the sensorless control of permanent magnet synchronous motor. The parameters of control system are obtained by trial and error method. The designed NTSMO not only ensures the fast response of the system, but also effectively weakens the chattering problem of the system. The adaptive observer filters out the high-order harmonics in the estimated value of the back-EMF signal and avoids the phase delay problem, which makes the rotor position estimation more accurate and suppresses the chattering.

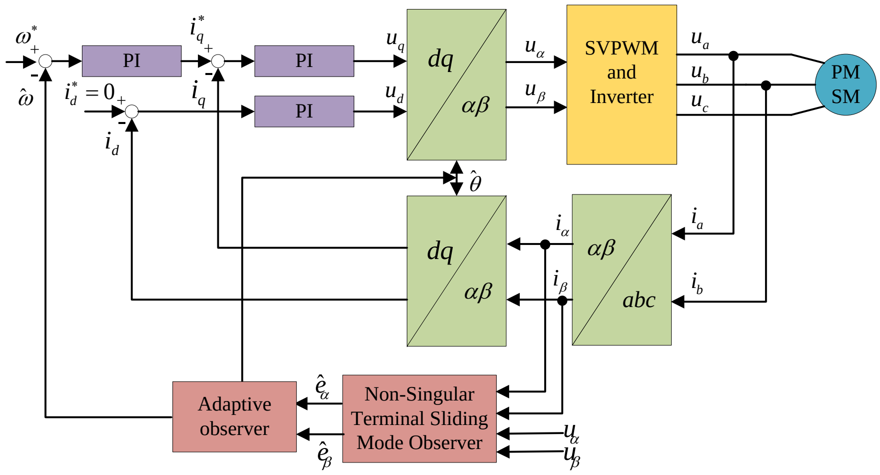

Figure 1. System structure diagram.

2.3. Numerical Analysis of Reaching Law

To verify the performance of the proposed sliding mode reaching law v_{sw}, a typical system (18) is taken as an example.

$$\dot{x} = Ax + Bu \tag{20}$$

The sliding mode surface of the system is chosen as $s = Cx$, then

$$\dot{s} = C\dot{x} \tag{21}$$

As shown in (13), the sliding mode reaching law is selected as $\dot{s} = -\frac{k}{\xi+\sigma^{|s|}}|s|^{\varpi}\mathrm{sgn}(s) - \frac{\varepsilon}{\xi+\sigma^{|s|}}s$, then

$$u = (CB)^{-1}[-CAx - \frac{k}{\xi+\sigma^{|Cx|}}|Cx|^{\varpi}\mathrm{sgn}(Cx) - \frac{\varepsilon}{\xi+\sigma^{|Cx|}}Cx] \tag{22}$$

where $x = [x_1\ x_2]^T$, x_1, and x_2 are the system state variable and the initial state of the system, $x(0) = [10\ \ 10]^T$, $X = x_1$, $k = 300$, $\xi = 0.5$, $\sigma = 0.01$, $\varpi = 0.5$, $\varepsilon = 50$. The simulation comparison results of the new reaching law and the exponential reaching law are shown in Figure 2 and Figure 3, respectively.

Figure 2 shows the numerical simulation of the performance of the new reaching law, and Figure 3 shows the numerical simulation of the performance of the exponential reaching law. By comparing the simulation results, it can be obtained that the new reaching law is better than the exponential reaching law in reaching speed and buffeting suppression; therefore, the new reaching law can shorten the time required for the system to reach the sliding mode surface, improve the speed of the system approaching the sliding mode surface, and reduce the chattering of the system.

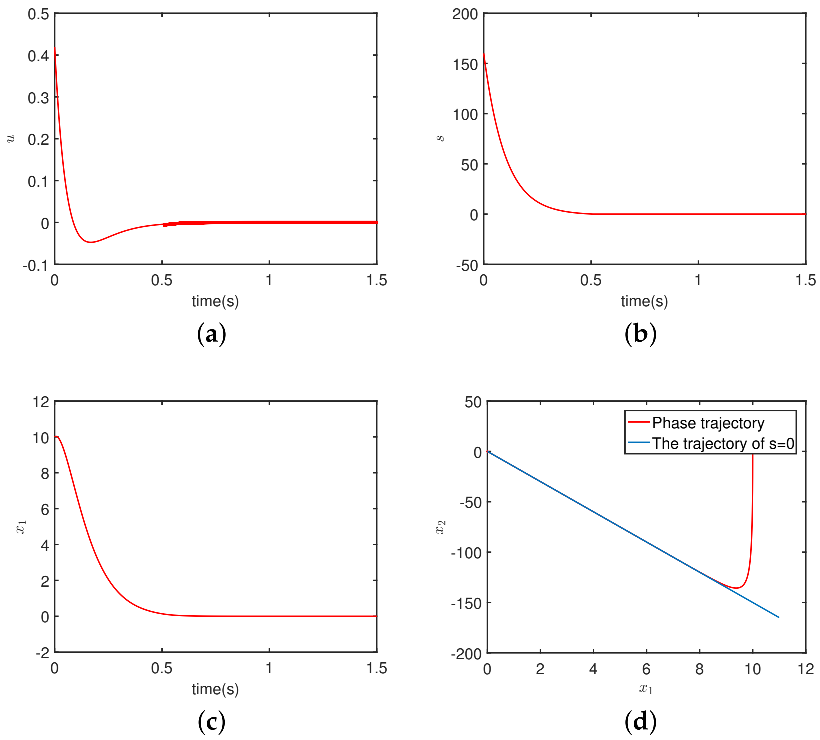

Figure 2. The performance of new reaching law. (**a**) Controller output; (**b**) approach time; (**c**) system status; (**d**) phase trajectory of sliding mode motion.

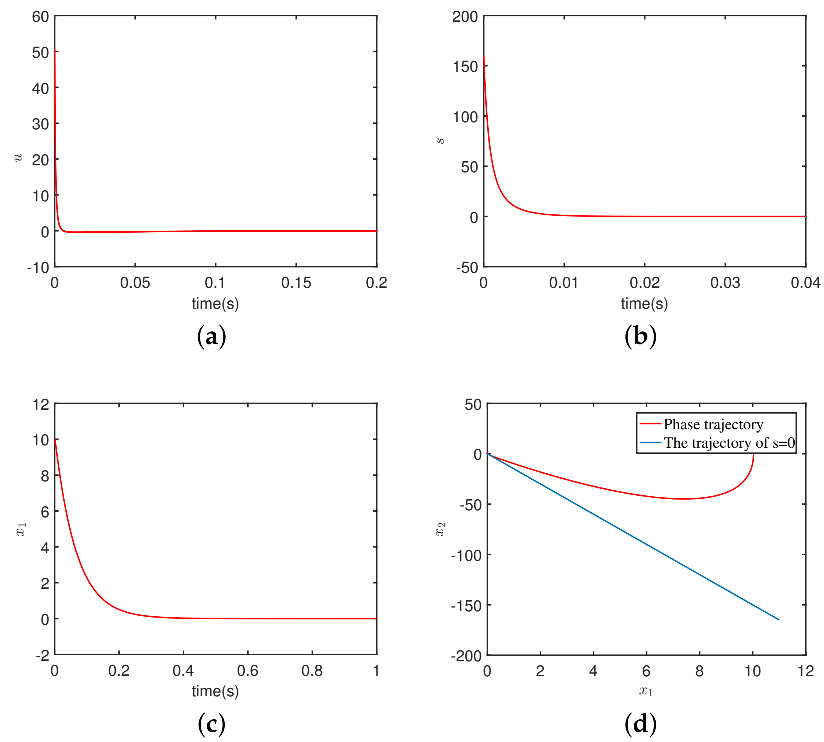

Figure 3. The performance of exponential reaching law. (**a**) Controller output; (**b**) approach time; (**c**) system status; (**d**) phase trajectory of sliding mode motion.

3. Experiment Analysis

In this part, to further verify the effectiveness of the proposed algorithm in this paper, the experimental verification was carried out on a motor-driven system; the experimental platform is shown in Figure 4. It mainly consists of the servo driver, PMSM, special motor control module, load control module, real-time simulator, and torque sensor. The control algorithm was compiled into the target code in MATLAB/Simulink. Then, it was downloaded to the real-time simulator. The motor was controlled by an RT-SIM software, which can observe the experimental waveform and data in real time. The experimental structure diagram of the drive system is shown in Figure 5. The motor parameters are shown in Table 1.

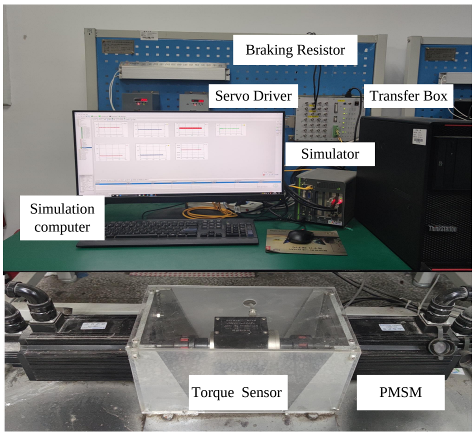

Figure 4. Experimental platform.

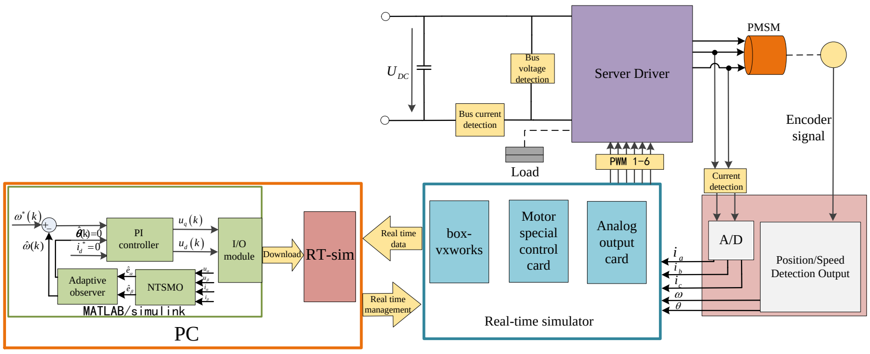

Figure 5. Experimental structure diagram of the drive system.

Table 1. Parameters of PMSM.

Description	Value	Unit
rated speed	1000	r/min
rated torque	14.5	$N \cdot m$
stator resistance	1.84	Ω
d-axis inductance	6.65	mH
q-axis inductance	6.65	mH
rotor flux	0.32	Wb
moment of inertia	0.0027	$Kg \cdot m^2$

To verify the control performance of nonsingular terminal sliding mode observer, the proposed method is compared with conventional sliding mode observer and super-twisting sliding mode observer [28]. The parameters of control system are obtained by trial and error method. The parameters of nonsingular terminal sliding mode observer are chosen as $k = 2$, $\xi = 0.5$, $\sigma = 0.01$, $\varpi = 0.5$, $\varepsilon = 0.5$, $\lambda = 0.5$, and $\beta = 5$. The mechanical sensors used in the experiment only record the actual rotor position and speed, and the detected information is not used for closed-loop control.

Firstly, the reference speed is given as 200 r/min. The estimated motor speed waveforms by the sensorless control algorithm are shown in Figure 6a. The actual motor speed waveforms by the mechanical sensors are shown in Figure 6b. The errors waveforms of actual speed and estimated speed are shown in Figure 6c. It can be seen from Figure 6, the fluctuations of observed speed with conventional SMO, FTSMO, and NTSMO are 9.4 r/min, 5.8 r/min, and 5.1 r/min, respectively. The fluctuations of actual speed are 8 r/min, 6 r/min, and 5 r/min, respectively. The fluctuations of speed error are 15 r/min, 12.5 r/min, and 11.2 r/min, respectively. The experiments are also completed with the reference speed of 600 r/min and 1000 r/min. The experimental results are shown in Figure 7 and Figure 8, respectively. Similarly, it can be seen from Figures 7 and 8 that when the speed is 600 r/min, the fluctuations of speed errors with conventional SMO, FTSMO, and NTSMO are 17.2 r/min, 13.3 r/min, and 8.7 r/min respectively. When the speed is 1000 r/min, the fluctuations of speed error with conventional SMO, FTSMO, and NTSMO are 23.2 r/min, 14.3r/min, and 12.6 r/min respectively. The detailed comparison is shown in Table 2. The experimental results show that the proposed NTSMO can reduce chattering and improve speed estimation accuracy.

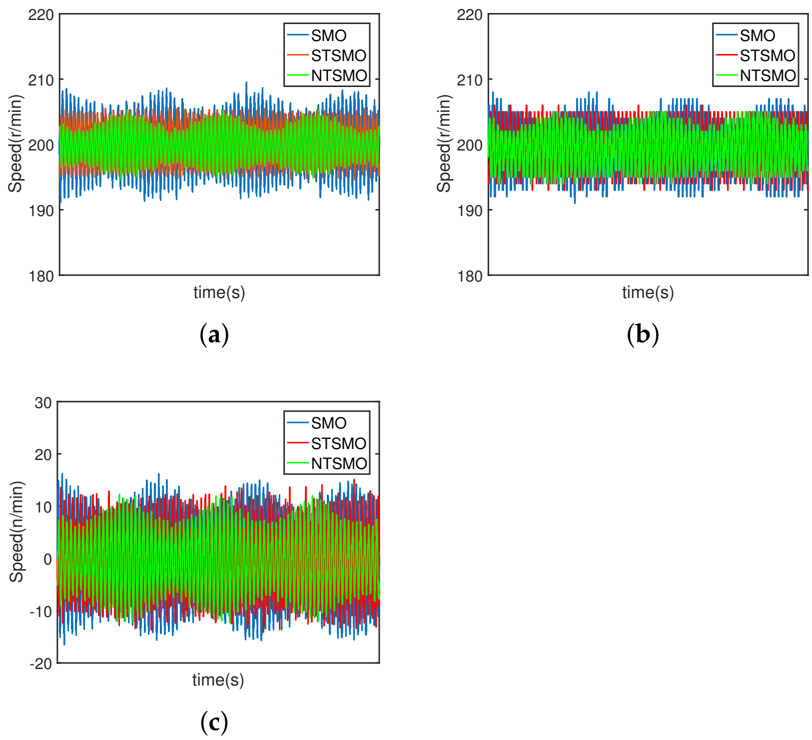

Figure 6. The speed waveforms with 200 r/min. (**a**) estimated speed; (**b**) actual speed; (**c**) speed error.

In addition, the rotor position waveforms with the proposed method are shown in Figures 9–11. Firstly, the reference speed is given as 200 r/min. The rotor position waveforms by the NTSMO are shown in Figure 9a. The rotor position error waveforms by the NTSMO are shown in Figure 9b. Because the rotor position changes periodically, rotor position tracking error will also appear a larger value periodically, but the actual rotor position tracking error is constant. As seen in Figure 9, the estimated rotor position can track the actual rotor position very well. The rotor position tracking error is 0.5 rad. The experiments were also completed with the reference speed of 600 r/min and 1000 r/min. It can be seen from Figures 10 and 11 that the rotor position error with 600 r/min is 0.08 rad and the rotor position error with 1000 r/min is 0.025 rad. It can be seen from the experimental results that the proposed method has good rotor position tracking performance. The phase delay problem caused by the low pass filter in the traditional method is solved.

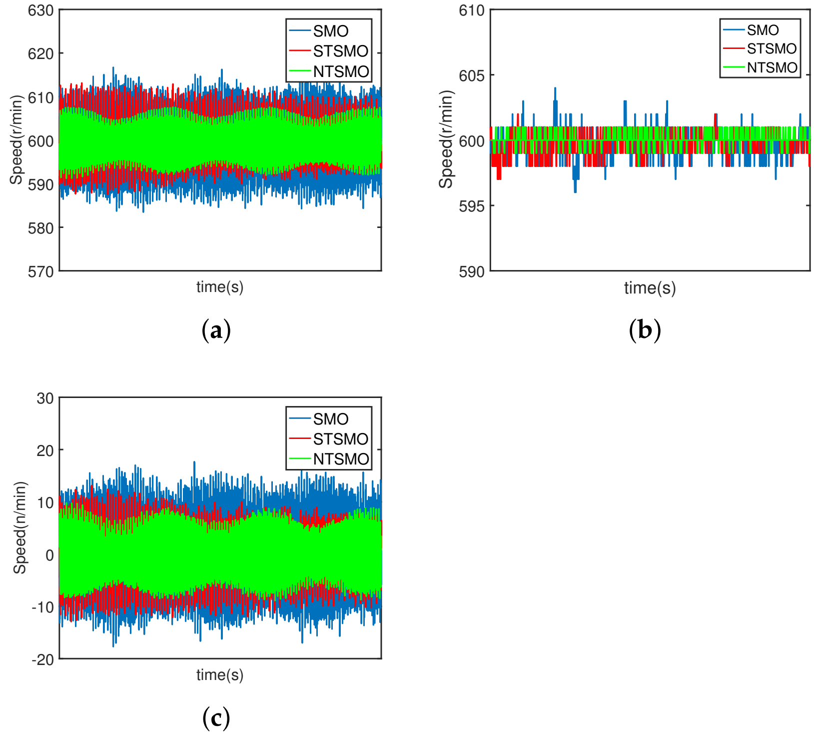

Figure 7. The speed waveforms with 600 r/min. (**a**) estimated speed; (**b**) actual speed; (**c**) speed error.

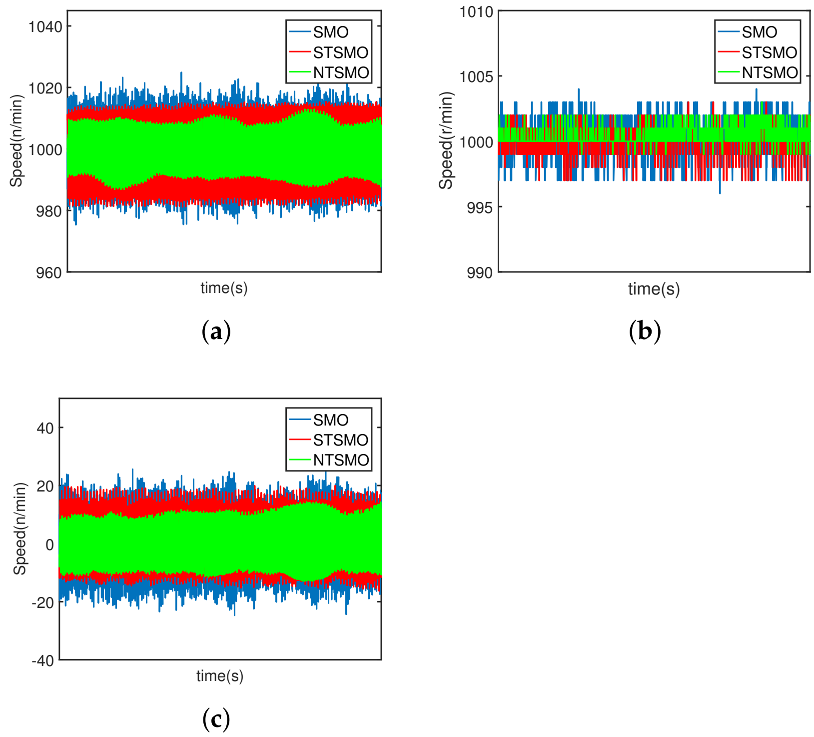

Figure 8. The speed waveforms with 1000 r/min. (**a**) estimated speed; (**b**) actual speed; (**c**) speed error.

Table 2. Detailed comparison of the three control algorithms at different speeds.

Speed	Method	Actual Speed (rpm)	Estimated Speed (rpm)	Speed Error (rpm)
200 rpm	SMO	−192∼208	−191.5∼209.3	−15.1∼14.8
	FTSMO	−194∼206	−194.1∼205.8	−12.5∼14.4
	NTSMO	−195∼205	−194.9∼205.1	−11.2∼11.3
600 rpm	SMO	−596∼604	−584.9∼615.1	−17.2∼17.3
	FTSMO	−593∼602	−588.2∼612.3	−13.3∼13.1
	NTSMO	−599∼601	−592.2∼607.5	−8.7∼8.7
1000 rpm	SMO	−996∼1004	−978.6∼1021.5	−23.2∼23.8
	FTSMO	−997∼1003	−981.3∼1013.2	−14.3∼18.8
	NTSMO	−999∼1002	−988.8∼1011.2	−12.6∼12.9

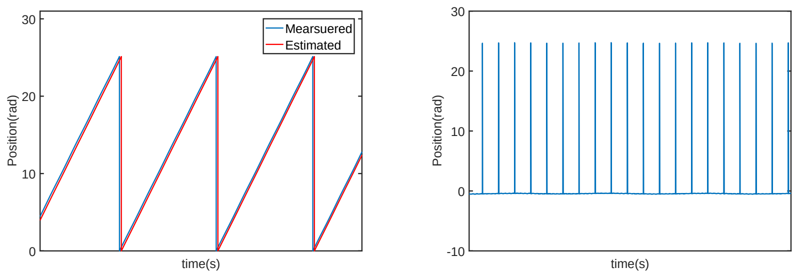

(**a**) (**b**)

Figure 9. The rotor position waveforms with 200 r/min. (**a**) Rotor position curve; (**b**) rotor position error curve.

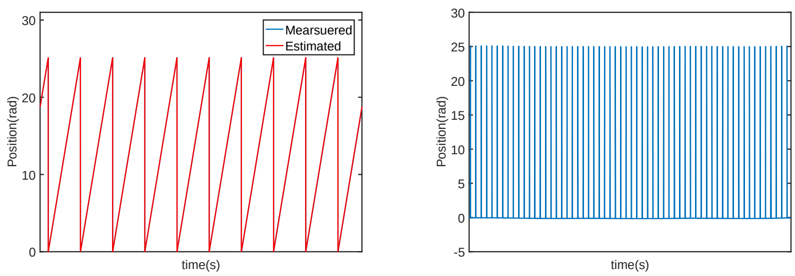

(**a**) (**b**)

Figure 10. The rotor position waveforms with 600 r/min. (**a**) Rotor position curve; (**b**) rotor position error curve.

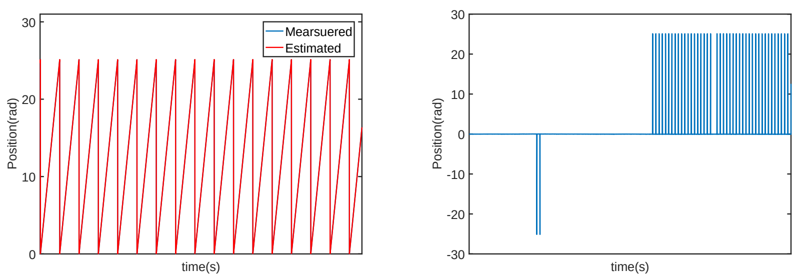

(**a**) (**b**)

Figure 11. The rotor position waveforms with 1000 r/min. (**a**) Rotor position curve; (**b**) rotor position error curve.

The back-EMF waveforms with the proposed method are shown in Figures 12–14. Firstly, the reference speed is given as 200 r/min. It can be seen from Figure 12a that the estimated back electromotive force is sinusoidal, but there are many harmonics in the signal and the curve is not smooth. It can be seen from Figure 12b that the filtered back electromotive force signal is relatively smooth. The experiments were also completed with the reference speed of 600 r/min and 1000 r/min. It can be seen from the experimental results that the proposed adaptive observer can filter out high-frequency chattering and harmonics of the estimated back-EMF and improve observation accuracy.

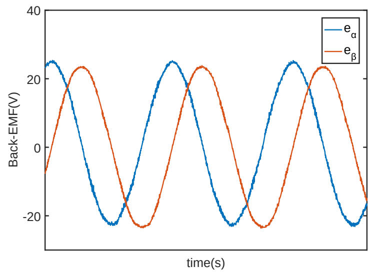

(**a**) (**b**)

Figure 12. The back-EMF waveforms with 200 r/min. (**a**) Before filtering; (**b**) after filtering.

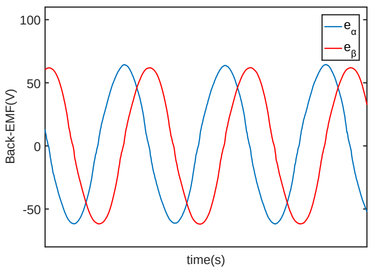

(**a**) (**b**)

Figure 13. The rotor position waveforms with 600 r/min. (**a**) Before filtering; (**b**) after filtering.

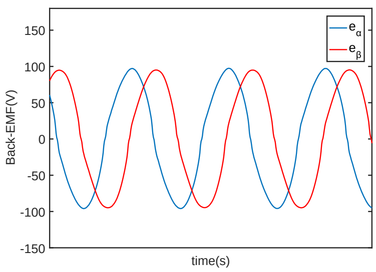

(**a**) (**b**)

Figure 14. The rotor position waveforms with 1000 r/min. (**a**) Before filtering; (**b**) after filtering.

To verify the control performance of the proposed observer with uncertain parameters, the reference speed is given as 600r/min, and the experiments were completed under different parameter conditions. Suppose $x = x_0(1 + \Delta x)$, $x = (R_s, L_s)$, where x_0 and Δx represent the nominal values and disturbance of the parameters, respectively. The results are shown in Figures 15–17. As seen in the figures, when the motor parameters are changed, the actual speed of the motor can track the reference speed well with the proposed sliding mode observer, and the system still has good speed control performance. The designed observer has strong robustness for the uncertain parameters.

To further verify the effectiveness of the proposed method under load disturbance. Figures 18 and 19 show the experimental waveforms and Q-axis current waveforms of different speeds under 1 Nm load disturbance, respectively. It can be seen from Figure 18a that the speed drop and recovery time of NTSMO at 200 r/min is 18 r and 0.2 s. When the load disturbance is removed, the speed fluctuation and recovery time is 18.5 r and 0.25 s. Similarly, it can be seen from Figure 18b,c that at 600 r/min and 1000 r/min, the speed drop and recovery time are 17.5 r, 0.2 s and 23.5 r, 0.25 s, respectively. When the load disturbance is removed, the speed fluctuation and recovery time is 18 r, 0.25 s and 24.5 r, 0.3 s, respectively. The experimental results show that the proposed observer can accurately estimate the rotor position and speed with load disturbance and the sensorless control system still has good speed control performance.

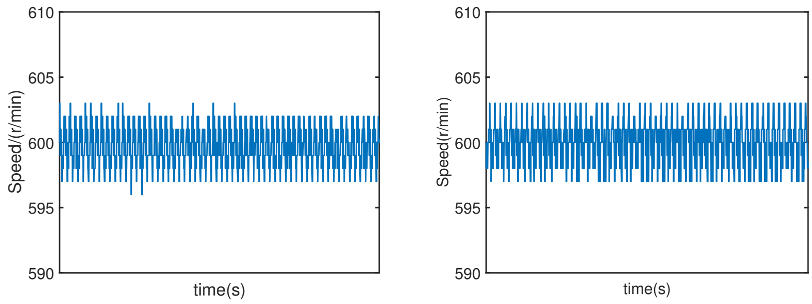

(**a**) (**b**)

Figure 15. The speed waveforms with a sudden change of parametric values. (**a**) $\Delta L_s = -50\%$; (**b**) $\Delta L_s = +50\%$.

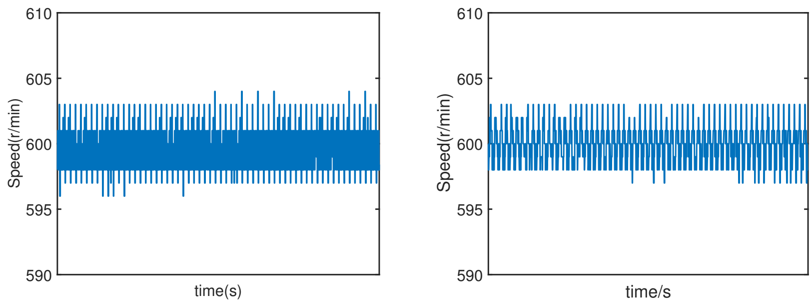

(**a**) (**b**)

Figure 16. The speed waveforms with a sudden change of parametric values. (**a**) $\Delta R_s = -50\%$; (**b**) $\Delta R_s = +50\%$.

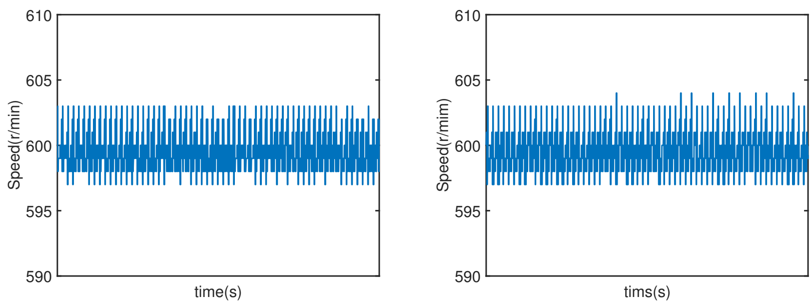

(**a**) (**b**)

Figure 17. The speed waveforms with a sudden change of parametric values. (**a**) $\Delta L_s = -50\%$, $\Delta R_s = -50\%$; (**b**) $\Delta L_s = +50\%$, $\Delta R_s = +50\%$.

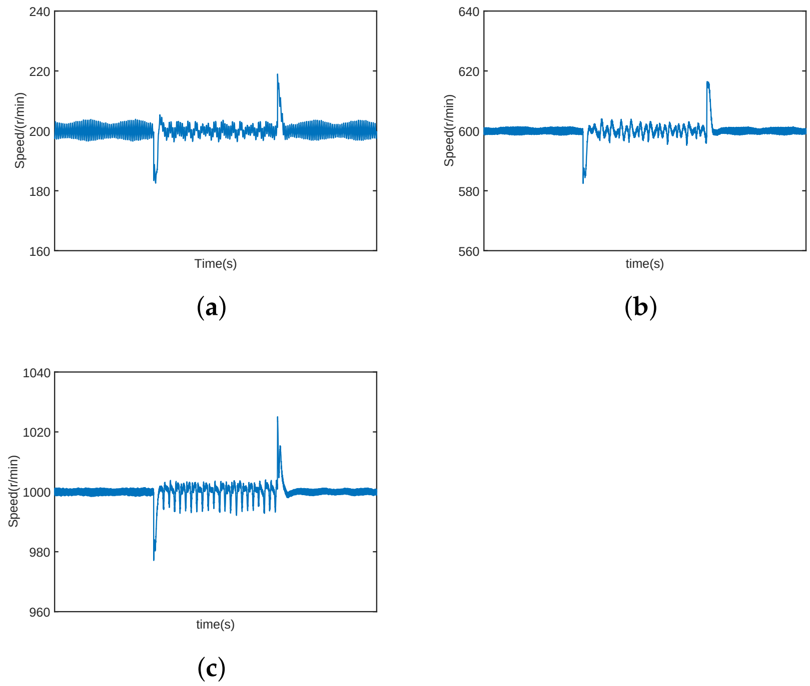

Figure 18. Experimental waveforms of different speeds under 1 Nm load disturbance. (**a**) 200 r/min; (**b**) 600 r/min; (**c**) 1000 r/min.

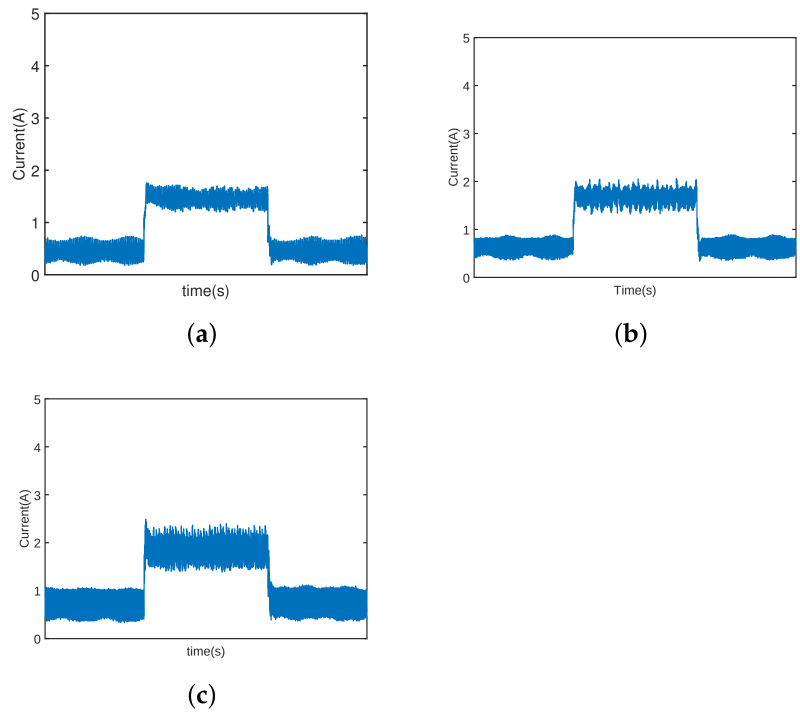

Figure 19. Q-axis current waveforms of different speeds under 1 Nm load disturbance. (**a**) 200 r/min; (**b**) 600 r/min; (**c**) 1000 r/min.

4. Conclusions

In this paper, a nonsingular terminal sliding mode observer and an adaptive observer are designed for the sensorless control system of a permanent magnet synchronous motor. Smooth back-EMF estimates are obtained by filtering the adaptive observer. Its stability was verified by Lyapunov criterion. The experimental results show that, compared with the conventional sliding mode observer and super-twisting sliding mode observer, the designed nonsingular terminal sliding mode observer has the advantages of high tracking accuracy, low chattering of rotational speed and low chattering of the counter electromotive force, and has strong robustness to load disturbance and better system stability.

Since the design of the sliding mode observer is based on the back-EMF model of the motor, this method is not suitable for zero and low-speed control. To better realize the sensorless speed control of PMSM, the control strategy considering the full speed range will be studied in the future.

Author Contributions: Conceptualization, X.L. and Y.Y.; methodology, Y.Y.; software, Y.Y.; validation, X.L.; formal analysis, Y.Y.; investigation, Y.Y.; resources, X.L.; data curation, X.L; writing—original draft preparation, Y.Y.; writing—review and editing, Y.Y; visualization, X.L; supervision, X.L.; project administration, X.L; funding acquisition, X.L. All authors have read and agreed to the published version of the manuscript.

Funding: This research was funded by the National Natural Science Foundation of China under Grant No. 52037005, in part by the China Postdoctoral Science Foundation under Grant No. 2018M632622, in part by the Science and Technology Support Plan for Youth Innovation of Universities in Shandong Province under Grant No. 2019KJN033.

Institutional Review Board Statement: Not applicable.

Informed Consent Statement: Not applicable.

Data Availability Statement: Not applicable.

Conflicts of Interest: The authors declare no conflict of interest.

Abbreviations

The following abbreviations are used in this manuscript:

NTSMO	nonsingular terminal sliding mode observer
EMF	estimate the back electromotive force
PMSM	permanent magnet synchronous motor
SMO	sliding mode observer
SMC	sliding mode control
VSI	voltage source inverter
STSMO	super-twisting sliding mode observer
FOTSM	full-order terminal sliding mode

References

1. Dianov, A.; Anuchin, A. Design of Constraints for Seeking Maximum Torque per Ampere Techniques in an Interior Permanent Magnet Synchronous Motor Control. *Mathematics* **2021**, *9*, 2785. [CrossRef]
2. Belkhier, Y.; Achour, A. An intelligent passivity-based backstepping approach for optimal control for grid-connecting permanent magnet synchronous generator-based tidal conversion system. *Int. J. Energy Res.* **2021**, *45*, 5433–5448. [CrossRef]
3. Xue, Z.; Li, L.; Wang, X.; Wang, X. A Sensorless Control Strategy for Permanent Magnet Synchronous Motor at Low Switching Frequency. *Electronics* **2022**, *11*, 1957. [CrossRef]
4. Yao, H.; Yan, Y.; Shi, T. A Novel SVPWM Scheme for Field-Oriented Vector-Controlled PMSM Drive System Fed by Cascaded H-Bridge Inverter. *IEEE Trans. Power Electron.* **2021**, *36*, 8988–9000. [CrossRef]
5. Xu, B.; Ma, J.; Wu, Q.; Qiu, L. Sensorless Control Strategy of Novel Axially Magnetized Vernier Permanent-Magnet Machine. *Energies* **2022**, *15*, 5470. [CrossRef]
6. Ye, S.; Yao, X. An Enhanced SMO-Based Permanent-Magnet Synchronous Machine Sensorless Drive Scheme With Current Measurement Error Compensation. *IET Electron. Power Appl.* **2021**, *9*, 4407–4419. [CrossRef]
7. Mai, Z. HF Pulsating Carrier Voltage Injection Method Based on Improved Position Error Signal Extraction Strategy for PMSM Position Sensorless Control. *IEEE Trans. Power Electron.* **2021**, *36*, 9348–9360. [CrossRef]
8. Lu, Q.; Wang, Y.; Mo, L.; Zhang, T. Pulsating High Frequency Voltage Injection Strategy for Sensorless Permanent Magnet Synchronous Motor Drives. *IEEE Trans. Appl. Supercond.* **2021**, *31*, 1–4. [CrossRef]
9. Liu, Z.; Chen, W. Research on an Improved Sliding Mode Observer for Speed Estimation in Permanent Magnet Synchronous Motor. *Processes* **2022**, *10*, 1182. [CrossRef]

10. Filho, C.J.V.; Xiao, D.; Vieira, R.P.; Emadi, A. Observers for High-Speed Sensorless PMSM Drives: Design Methods, Tuning Challenges and Future Trends. *IEEE Access* **2021**, *9*, 56397–56415. [CrossRef]
11. Shao, Y.; Wang, B.; Yu, Y.; Dong, Q.; Tian, M. An Integral Sliding Mode Back-EMF Observer for Position-Sensorless Permanent Magnet Synchronous Motor Drives. In Proceedings of the 2019 22nd International Conference on Electrical Machines and Systems (ICEMS), Harbin, China, 11–14 August 2019; pp. 1–5.
12. Wang, Y.; Feng, Y.; Zhang, X.; Liang, J. A New Reaching Law for Antidisturbance Sliding-Mode Control of PMSM Speed Regulation System. *IEEE Trans. Power Electron.* **2020**, *35*, 4117–4126. [CrossRef]
13. Tang, Y.; Xu, W.; Liu, Y.; Dong, D. Dynamic Performance Enhancement Method Based on Improved Model Reference Adaptive System for SPMSM Sensorless Drives. *IEEE Access* **2021**, *9*, 135012–135023. [CrossRef]
14. Xu, W.; Jiang, Y.; Mu, C.; Blaabjergc, F. Improved Nonlinear Flux Observer-Based Second-Order SOIFO for PMSM Sensorless Control. *IEEE Trans. Power Electron.* **2019**, *34*, 565–579. [CrossRef]
15. Cui, J.; Xing, W.; Qin, H.; Hua, Y. Research on Permanent Magnet Synchronous Motor Control System Based on Adaptive Kalman Filter. *Appl. Sci.* **2022**, *12*, 4944. [CrossRef]
16. Novak, Z.; Novak, M. Adaptive PLL-Based Sensorless Control for Improved Dynamics of High-Speed PMSM. *IEEE Trans. Power Electron.* **2022**, *37*, 10154–10165. [CrossRef]
17. Ma, Z.; Zhang, X. FPGA Implementation of Sensorless Sliding Mode Observer with a Novel Rotation Direction Detection for PMSM Drives. *IEEE Access* **2018**, *6*, 55528–55536. [CrossRef]
18. Nicola, M.; Nicola, C.-I.; Selișteanu, D. Improvement of PMSM Sensorless Control Based on Synergetic and Sliding Mode Controllers Using a Reinforcement Learning Deep Deterministic Policy Gradient Agent. *Energies* **2022**, *15*, 2208. [CrossRef]
19. Cui, J.; Xing, W.; Qin, H.; Hua, Y. Ghoneim, Robust interconnection and damping assignment energy-based control for a permanent magnet synchronous motor using high order sliding mode approach and nonlinear observer. *Energy Rep.* **2022**, *8*, 1731–1740.
20. Li, L.; Zhang, Z.; Wang, C. A flexible current tracking control of sensorless induction motors via adaptive observer. *ISA Trans.* **2019**, *93*, 180–188. [CrossRef]
21. Repecho, V.; Waqar, J.; Biel, D. Zero speed sensorless scheme for PMSM under decoupled sliding mode control. *IEEE Access* **2018**, *6*, 55528–55536.
22. Liang, D.; Li, J.; Qu, R.; Kong, W. Adaptive Second-Order Sliding-Mode Observer for PMSM Sensorless Control Considering VSI Nonlinearity. *IEEE Trans. Power Electron.* **2018**, *3*, 8994–9004. [CrossRef]
23. Gong, C.; Hu, Y.; Gao, J.; Wang, Y.; Yan, L. An Improved Delay-Suppressed Sliding-Mode Observer for Sensorless Vector-Controlled PMSM. *IEEE Trans. Ind. Electron.* **2020**, *67*, 5913–5923. [CrossRef]
24. Zhou, M.; Cheng, S.; Feng, Y.; Xu, W.; Wang, L.; Cai, W. Full-Order Terminal Sliding-Mode-Based Sensorless Control of Induction Motor With Gain Adaptation. *IEEE J. Emerg. Sel. Top. Power Electron.* **2022**, *10*, 1978–1991. [CrossRef]
25. Yuan, Q.; Yang, Y.; Wu, H.; Wu, H. Low Speed Sensorless Control Based on an Improved Sliding Mode Observation and the Inverter Nonlinearity Compensation for SPMSM. *IEEE Access* **2020**, *8*, 61299–61310. [CrossRef]
26. Yin, Z.; Zhang, Y.; Cao, X.; Yuan, D.; Liu, J. Estimated Position Error Suppression Using Novel PLL for IPMSM Sensorless Drives Based on Full-Order SMO. *IEEE Trans. Power Electron.* **2022**, *37*, 4463–4474. [CrossRef]
27. Yang, C.; Ma, T.; Che, Z.; Zhou, L. An Adaptive-Gain Sliding Mode Observer for Sensorless Control of Permanent Magnet Linear Synchronous Motors. *IEEE Access* **2018**, *6*, 3469–3478. [CrossRef]
28. Zhao, Y.; Yu, H.; Wang, S. An Improved Super-Twisting High-Order Sliding Mode Observer for Sensorless Control of Permanent Magnet Synchronous Motor. *Energies* **2021**, *14*, 6047. [CrossRef]
29. Zhang, Y.; Jin, J.; Huang, L. Model-Free Predictive Current Control of PMSM Drives Based on Extended State Observer Using Ultralocal Model. *IEEE Trans. Ind. Electron.* **2021**, *68*, 993–1003. [CrossRef]
30. Lu, H.; Wu, J.; Li, M. A new sliding mode observer for the sensorless control of a PMLSM. In Proceedings of the 2017 29th Chinese Control And Decision Conference (CCDC), Chongqing, China, 28–30 May 2017; pp. 5364–5369.
31. Jayaramu, M.L.; Suresh, H.N.; Bhaskar, M.S. Real-Time Implementation of Extended Kalman Filter Observer With Improved Speed Estimation for Sensorless Control. *IEEE Access* **2021**, *9*, 50452–50465. [CrossRef]
32. Lee, H.; Lee, J. Design of Iterative Sliding Mode Observer for Sensorless PMSM Control. *IIEEE Trans. Control. Syst. Technol.* **2013**, *21*, 1394–1399. [CrossRef]
33. Yu, X.; Feng, Y.; Man, Z. Terminal Sliding Mode Control—An Overview. *IEEE Trans. Ind. Electron.* **2021**, *2*, 36–52. [CrossRef]
34. Song, L.; Huang, J.; Liang, Q.; Nie, L.; Liang, X.; Zhu, J. Trajectory Tracking Strategy for Sliding Mode Control with Double Closed-Loop for Lawn Mowing Robot Based on ESO. *IEEE Access* **2022**, 1–16. [CrossRef]
35. Chang, X.; Bloomberg; Liu, L. Sensorless control of permanent magnet synchronous motor with a novel non-singular terminal sliding mode observer. *J. Jiaotong Univ.* **2016**, *50*, 85–91.